SVM-based Classification of Multi-temporal Sentinel-2 Imagery of Dense urban Land Cover

Yash Khurana
Vellore Institute of Technology University
Pramod Kumar Soni (Pramod.soni@jaipur.manipal.edu)
manipal university jaipur
Devershi Pallavi Bhatt
manipal university jaipur

Research Article

Keywords: Sentinel-2, urban land cover and land use, SVM, RBF, and polynomial kernel

Posted Date: November 22nd, 2022

DOI: https://doi.org/10.21203/rs.3.rs-2259178/v1

Additional Declarations: No competing interests reported.

Version of Record: A version of this preprint was published at Earth Science Informatics on April 15th, 2023. See the published version at https://doi.org/10.1007/s12145-023-01008-5.

Abstract

The technological breakthrough and the availability of multispectral remote sensing data have given rise to an ambitious challenge for the classification of the multispectral images accurately to support administrative bodies in decision-making. In this paper, the multi-temporal medium resolution Sentinel-2 imagery of the densely populated urban area of Delhi-NCR is classified using SVM into five different land cover classes, namely water bodies, barren land, vegetative region, road network, and residential areas. Further, the effect of different kernel functions of SVM on land cover classification performance is contrasted and the radial basis function (RBF) leads to the best results. The experimental results are compared with the maximum likelihood classification (MLC) method on different evaluation metrics. The SVM with RBF kernel shows promising improvements in the overall accuracy by 10 percent relative to the polynomial kernel and by 3 percent compared to MLC. The analysis of multitemporal spectral imagery of the study area reflects the increase in a built-up area (road network, Buildings), water bodies, and decrement in the area of barren land and vegetation.

1. Introduction

Before the invention of remote sensing technology (RST), the main source of information about the land surface was the data collected by surveying the geographical site physically. Due to the large land cover area, it is difficult and time-consuming to physically visit all the places and the information obtained is also subjected to various errors arising from human intervention. The evolution of RST and improvements in computing power have facilitated the extraction of meaningful information about cartographic objects from remote sensing data covering a large land cover area efficiently and cost-effectively as compared to manual observation. Additionally, it has also facilitated the monitoring of land surface at regular intervals that help in change detection in land cover and land use and supports various applications related to urban landscape planning and environment such as vegetation cover mapping(Nizalapur et al. 2011), urban planning(Stefanov et al. 2001), monitoring water bodies (Steinhausen et al. 2018), agricultural field (Sishodia et al. 2020; Magno et al. 2021), disaster management (Frazier et al. 2012), road network extraction (Miao et al. 2015; Liu et al. 2016), encroachment detection (Shekede et al. 2015) and building detection (Sumer and Turker 2013; Rottensteiner et al. 2014). Remote sensing data of varying spatial resolution can be obtained from satellites such as Landsat (Goldblatt et al. 2018), MODIS(Frazier et al. 2012), SPOT (Huang and Siegert 2006), Sentinel (Spoto et al. 2012), etc. The land cover information extraction from satellite imagery heavily depends on the type of sensor, spatial resolution provides by satellites. Based on its spatial resolution, satellite imagery can be categorized into various types, namely low-resolution (> 30m), medium-resolution (5-30m), high-resolution(1-5m), and very high-resolution (< 1 m) imagery (Sheykhmousa et al. 2020). The low-resolution images are primarily suitable for extracting information and detecting the change in large land areas such as forest cover, agriculture, barren land, water bodies, etc. Medium-resolution imagery contains more information about the land cover as compared to low-resolution imagery and is ideal for obtaining contextual objects like large building structures, highways, and change detection in urban and semi-urban settlements. The high-resolution and very high-resolution imagery have more precise information about land cover and different contextual objects as compared to low and medium resolution and are utilized for a more intricate extraction process.

Land cover information extraction from the urban landscape is a challenging task due to the presence of complex heterogeneous objects and low variation in spectral properties. Several techniques have been designed for the information extraction about different contextual urban objects from the satellite of varying resolution (Stefanov et al. 2001; Zhu et al. 2012; Isaac et al. 2017). An expert urban land cover information extraction system based on MLC and texture analysis has been designed to classify the urban land cover into different classes, namely vacant, asphalt, vegetation and residential from Landsat thematic map imagery of 28.5 m resolution (Stefanov et al. 2001). The urban land cover information about 17 different classes like orchards, deep water, shallow water, commercial buildings, etc., have been extracted from PALSAR data using a random forest classifier (Zhu et al. 2012). A two-stage competitive multiscale object-based segmentation method has been designed to classify the high-resolution aerial imagery of urban segments into three different segments (Johnson 2013). However, the performance of the method suffers to some extent as real-world objects don't have any regular shape. The multi-sensory multi-spectral urban data has been classified into 20 different land cover classes utilizing deep learning architecture (Xu et al. 2019). SVM has been effectively employed to classify the urban land cover from low-resolution imagery of Landsat-5 having a maximum resolution of 120 m into 8 different classes, with satisfactory performance in extensive urban and urban segments as compared to other classes (Yang 2011). An automated land cover information extraction technique based on the random forest has been designed to classify the multi-temporal Sentinel-1 and 2 satellite imagery of Iran into 13 different classes, but the accuracy deteriorates in building structure information extraction (Ghorbanian et al. 2020). An ensemble learning method using Adaboosted random forest has been designed to detect urban land cover information from aerial ortho imagery (Isaac et al. 2017). A pixel-based (SVM) and object (SVM and decision tree) based classifier has been designed to classify the urban area of SPOT imagery into various classes (Jebur et al. 2014). Similarly, the classification performance of different machine learning algorithms has been evaluated on the Boreal landscape from Sentinel-2 imagery (Abdi 2020).

Urbanization is a dynamic process and the Spatio-temporal pattern of urban land cover must be monitored which can be achieved by RST. Due to the rapid industrialization during the last three decades, the population density of the Delhi-NCR approximately doubles from 1991 to 2011(census of India,2022). These factors have led to the alteration of LCLU resulting in a change in administrative authorities' policies (transportation, education, health, industry, etc.). The main reason for selecting the study area as it has an ideal complex scene to analyze the performance of SVM kernel functions in the urban landscape. The earlier classification studies of the study area primarily deal with the use of low-resolution Landsat satellite imagery and are unable to provide a precise classification of the urban landscape as a lot of urban components have a size smaller than the spatial resolution of the imagery (Dutta et al. 2020; Naikoo et al. 2020). The Sentinel-2 imagery provides a comparatively high 10 m resolution, and its radiometry encompasses vegetation red edge bands (Abdi 2020). These characteristics of Sentinel imagery make it ideal for LCLU mapping and monitoring tasks.

To handle the aforementioned issues, in this work the multispectral Sentinel-2 imagery of the complex urban landscape of the Delhi-NCR region as shown in Fig. 1 is classified into different classes namely: water bodies, vegetation, road network, barren land, and Residential/Buildings using SVM. Further, the classification performances of polynomial and radial basis kernels are thoroughly analyzed on different evaluation metrics. It should be emphasized that since the selection of kernel parameters affects the generalization ability of SVM, determining their optimal parameters is regarded as crucial for the success of classification. The performance of SVM is compared with the MLC method. The main objectives of this paper are as follows: (1) to classify the urban land cover using SVM (2) to investigate the performance of SVM on different parameters (3) to perform a cross-comparison of the classification accuracies with other classification methods.

The remaining paper includes four other sections. The study area and dataset used are described in Section 2 followed by the description of the method consisting of preprocessing and formulation of SVMs used for multiclass classification in Section 3. The experimental results and comparative analysis is discussed in Section 4. Finally, the conclusions are drawn in Section 5.

2. Study Area And Dataset

The study area as shown in Fig. 1 25x 25 km^2 situated in the National Capital Territory Delhi with adjoining districts of Haryana (only the western area of Delhi and adjoining districts of Haryana). It is geographically located from 76^{0}58'4E to 77^{0}6'34 E longitude to 28^{0}33'52" N 28^{0}41'31" N latitudes. The study area is densely populated with large residential structures, commercial complexes, barren land in outer regions of Delhi, and industrialization units as well. The information extraction from such types of terrain using medium-resolution data is a challenging task. In this work multispectral Sentinel-2 A (The European Space Agency) level 1C products were obtained from USGS (2020). The sentinel-2 is a polar-orbiting multi-spectral imaging mission consisting of twin constellations of Sentinel – 2A and 2B It has a swath width of 290 km and a revisit time of 5 days. the detailed specification of spectral bands is described in Table 1 and the relationship between spectral bands and spatial resolution is shown in Fig. 2. The main objective of the Sentinel-2 mission is to provide high-resolution data as compared to the Landsat program to monitor LCLU classification, information extraction, change detection, disaster management, etc. In this work, multi-temporal data of pre (April) and post-Monson (September) seasons of different years 2022 and 2020 of Sentinel-2 has been used for the study of the land cover classes. The imagery acquired in September 2020 is categorized as Test case 1 and the imagery acquired in April 2022 as Test case 2.

Figure 2. Relationship between spatation resolution and spectral bands

Table 2
Sentinel-2 data bands and other details

Spectral band	Spatation resolution in metres	Center wavelength in nm	Bandwidth in nm
Band-2	10	490	65
Band-3	10	560	35
Band-4	10	665	30
Band8	10	842	115
Band5	20	705	15
Band 6	20	740	15
Band 7	20	783	20
Band 8A	20	865	20
Band 11	20	1610	90
Band 12	20	2190	180
Band 1	60	442.7	20
Band 9	60	945	20
Band 10	60	1375	30

3. Method

This section discusses the preprocessing, selection of training and validation samples, and SVM formulation used for the classification of multispectral imagery of the study area.

3.1 Preprocessing of multispectral Sentinel imagery

The sentinel-2 satellite produces Level1C data in JPG2000 format which suffers from noise during image acquisition from different sources such as thermal, atmospheric disturbance, etc,. To eliminate the noise the Level1C data is preprocessed according to the L2 algorithm defined in the Sen2Cor toolbox with SNAP tool version 8.0. The L2 algorithm generates a pixel classification map and performs atmospheric correction which transforms the top of atmosphere reflectance into the bottom of sphere reflectance. The true color imagery of 10 m resolution is obtained by composting

Bands 2, 3, and 4. To enhance the contrast between different contextual objects of the dense urban area image, histogram equalization is performed (Demirel et al. 2010).

3.2 SVM formulation for multiclass Land cover classification

SVM(Cortes and Vapnik 1995) is a non-parametric statistical theory-based classification technique used to solve problems that involve classification(Abdollahi et al. 2018; Rana and Venkata Suryanarayana 2020) and non-linear regression tasks(Norinder 2003; Mukkamala et al. 2005). The main objective of the SVM is to determine a hyperplane that optimally discriminates (minimizes the misclassifications) the training dataset into the required number of classes and its generalization capability is tested with testing datasets. SVM is used in a wide range of applications such as image classification(Miao et al. 2015), medical (Huang et al. 2012), and remote sensing (Demirel et al. 2011), pattern recognition(Chen and Xie 2007) ,etc. In the last two decades, SVM has been widely used by researchers for the classification of remote sensing data of varying spatial resolution for extracting information about different contextual objects like roads, buildings, land cover, vegetation, etc (Mukhopadhyay and Maulik 2009; Cheng et al. 2014; Wang et al. 2017; Lantzanakis et al. 2020).

For performing binary classification task SVM in q dimensional space having k training sample described as,

$$\{x_i, y_i\}\ i = 1{,}2\ldots\ldots\ldots\ldots k$$

1

where $x \in R^q \text{ and } y \in \{-1, +1\}$attempts to find a hyperplane. For linear separable case hyperplane can be defined as,

$$w.\,x_i + b \geq +1,\ \forall y = +1$$

2

$$w.\,x_i + b \leq -1,\ \forall y = -1$$

3

Where w and b denote the normal to the hyperplane and bias respectively. Eq. (3) and Eq. (4) can be merged and can be expressed as,

$$y_i(w.\,x_i + b) - 1 \geq 0$$

4

and this can be formulated into an optimization problem described as,

$$min\left|\frac{1}{2}||\,w||^2\right|$$

5

In the case of the non-linear separable case, the slack variable ξ is introduced and can be described as,

$$min\left\{\frac{1}{2}||\,w||^2 + P\sum\nolimits_{i=1}^{r}\xi_i\right\}$$

6

Where $P\sum_{i=1}^{r}\xi_i$ is the penalty term and subject to constraints,

$$y_i(wxi+b)\geq 1-\xi_i,\ \xi_i\geq 0$$

7

And in higher dimensional space (H) the linear SVM classifier is mapped into H by using a non-linear mapping function (φ) and the SVM classifier takes the following form,

$$f\left(x\right)=sign\left[\sum_{i=1}^{r}a_iy_i.\,K(x,x_i)+b\right]$$

8

Where $K(x,x_i)=(\varphi(\,x).\,\varphi(x_i\,))$ and a_i is the Lagrange multiplier. The computation involved in this mapping is reduced by the kernel trick which enables the input points to spread over such that the hyperplane can be fitted(Dixon and Candade 2008). SVM supports the following kernels linear, polynomial, RBF and Sigmoid. In LCLU classification of satellite imagery polynomial kernel $((\,x,y)+a)^d)$ and RBF kernel $e^{-y||(x-x_i)||^2}$ are widely used. In RBF kernel regularization parameter (C) and kernel, width (λ) while in case of polynomial kernel parameter (C) and degree of the polynomial kernel (d) is required. In the present work, the hyperparameters are selected by the k-fold cross-validation process.

As discussed above, SVMs are intrinsically binary classifiers. But, the LCLU classification of multispectral imagery involves multiclass classification. To handle this situation one against one (OAO) and one against all (OAA) which are ensembles of binary SVM (Mathur and Foody 2008).

(a) OAA ensembles: Let $\alpha=\{\alpha_1,\alpha_2,\alpha_3.\dots\dots..\alpha_n)$ be the collection of land cover classes then OAA construct a set of binary classfiers$\{f_1,f_2,f_3.\dots\dots.f_n\}$. Each of f_i where $i=1,2,\dots\dots\dots..,n$is competent individually to distinguish class $\alpha_i$from the rest of the classes $(\alpha-\alpha_i)$. An unknown pattern is assigned to the class by selecting maximum decision value of $f_i(x)$which can be calculated as follows,

$$a*=\begin{matrix}\arg\max\\ i\end{matrix}\ f_i(x)=\left\{\sum_{i=S}a_i^*y_iK(x_i,x)+b*\right\}$$

9

(b) OAA ensembles: in this strategy, each enseable discriminate between two classes $\alpha_i$and $\alpha_j$through decision function $f_{ij}(x)$and involves $n(n-1)/2$binary classifiers. All decisions are combined to find a score function $S_i(x)$for each class and the maximum score for a particular class is calculated as follows,

$$a*=\begin{matrix}\arg\max\\ i\end{matrix}\ f_i(x)=\left\{S_i(x)=sign\{f_{ij}(x)\}\right\}.$$

10

In this work, SVM based on OAO ensembles is used for the multiclass classification of Sentinel-2 imagery into different LCLU classes.

3.3 Selection of training and testing samples

For performing SVM based classification of land cover, the training and testing samples of each class are required which are collected by manual interpretation of true colour sentinel imagery by matching with Google earth imagery. The arbitrary number of pixels between (100–150 pixels) of each class are selected for training. For assessing the accuracy of classification results, the different number of pixels are selected for the Sentinel imagery of 2020 and 2022 as described in Table 2.

Table 2
validation Samples (pixels) for multi-temporal Sentinel-2 imagery

Class	Test case 1	Test case 2
Road Network	334	501
Vegetation	313	366
Barren Land	381	523
Water bodies	383	519
Residential/Buildings	350	506

4. Experimental Results And Comparative Analysis

This section discusses various experimental results of the classification of the multi-temporal Senitnel-2 imagery categorized as test case 1and test case 2. The results are evaluated on different evaluation metrics and finally the experimental results are compared with well known parameteric method (MLC).

4.1 Evluation metrics

The classification performance of SVM is evaluated using several metrics obtained from cross-tabulated data (error matrix). Which includes overall accuracy (OAC), producer accuracy (PAC), user's accuracy(UAC) and Kohen's Kappa (KPS) (Fung and Ledrew 1988; Foody 2002). The PAC is the number of correctly predicted samples divided by the total number of samples of a particular class and is a measure of the error of omission which can be calculated from the error matrix as,

$$UAC = \frac{X_{ii}}{\sum X_{+i}} * 100$$

11

The UAC measures the accuracy from the point of view of the user for a particular class. it is the number of correctly classified samples divided by total samples and measures the error of commission which can be calculated as,

$$PAC = \frac{X_{ii}}{\sum X_{i+}} * 100$$

12

The OAC measures the overall accuracy of classification i.e., correctly classified samples divided by the total number of samples and can be calculated as,

$$OAC = \frac{\sum_{i=1}^{n} X_{ii}}{\sum_{i=1}^{n} X_{ii}} * 100$$

13

The KPS(Cohen 1960) is an agreement between model and expected values, it covers both errors of commission and omissions errors. KPS depicts the performance of classification as compared to reference data and can be calculated as,

$$KPS = \frac{N \sum_{i=1}^{n} x_{ii} - \sum_{i=1}^{n} x_{i+} x_{+i}}{N^2 - \sum_{i=1}^{n} x_{i+} . x_{+i}}$$

14

4.2 Experimental results and comparative analysis

This section discusses the experiments performed on multi-temporal multispectral Sentinel-2 imagery using SVM and the performance of RBF and polynomial is kernel is evaluated. Furthermore, the classification performance of SVM is compared with parametric and widely used MLC classifiers.

The experimental results on the imagery of Test case 1 using SVM with RBF and polynomial kernel are shown in Fig. 2 and Fig. 3. The performance of these kernels is calculated on various accuracy assessment metrics PAC, UAC, OAC and KPS, and the results are shown in Tables 3 and 4. The RBF kernel has better OAC and KPS values as compared to the polynomial kernel which is reflected in experimental results.

Table 3
Error matrix of Test case 1 imagery with RBF kernel

	Road Network	**Vegetation**	**Barren Land**	**Water bodies**	**Residential/Buildings**	**Total**	**User's accuracy**
Road Network	328	0	6	1	0	335	97.91
Vegetation	1	313	0	0	0	314	99.68
Barren Land	1	0	360	0	5	366	98.36
Water bodies	1	0	0	382	0	383	99.74
Residential/Buildings	3	0	15	0	345	363	95.04
Total	334	313	381	383	350	1761	
Producer's accuracy	98.2	100	94.49	99.74	98.57		
Overall Accuracy 98.13							
Overall kappa 0.9765							

Table 4
Error matrix of Test case 1 imagery with Polynomial Kernel

	Road Network	**Vegetation**	**Barren Land**	**Water bodies**	**Residential/Buildings**	**Total**	**User's accuracy**
Road Network	328	198	6	1	0	533	61.54
Vegetation	1	115	0	0	0	116	99.14
Barren Land	1	0	360	0	5	366	98.36
Water bodies	1	0	0	382	0	383	95.04
Residential/Buildings	3	0	15	0	345	363	99.74
Total	334	313	381	383		1761	
Producer's accuracy	98.2	36.74	94.49	99.74	98.57		
Overall Accuracy 86.88							
Overall kappa 0.8355							

To measure the temporal effects on classification performance the experiments are performed on Test case 2 imagery of the study area with RBF and polynomial kernels. The classification map of imagery of Test Case 2 are shown in Figs. 4 and 5 and the accuracy assessment on different parameters is presented in Tables 5 and 6.

Table 5
Error matrix of Test case 2 imagery with RBF kernel

	Road Network	**Vegetation**	**Barren Land**	**Water bodies**	**Residential/Buildings**	**Total**	**User's accuracy**
Road Network	486	1	0	1	20	508	95.67
Vegetation	0	360	0	0	1	361	99.72
Barren Land	12	0	468	0	16	496	94.35
Water bodies	0	4	0	499	0	503	99.20
Residential/Buildings	2	1	34	0	463	500	92.60
Total	500	366	502	500	500	2368	
Producer's accuracy	97.20	98.36	93.23	99.80	92.60		
Overall Accuracy :96.11							
Overall kappa 0.9513							

Table 6
Error matrix of Test case 2 imagery with polynomial kernel

	Road Network	**Vegetation**	**Barren Land**	**Water bodies**	**Residential/Buildings**	**Total**	**User's accuracy**
Road Network	490	39	0	0	28	557	87.97
Vegetation	0	300	0	0	1	301	99.67
Barren Land	7	0	475	0	19	501	94.81
Water bodies	3	27	0	500	0	530	94.34
Residential/Buildings	0	0	27	0	452	479	94.36
Total	500	366	502	500	500	2368	
Producer's accuracy	98	81.97	94.62	100	90.40		
Overall Accuracy : 93.62							
Overall kappa 0.9199							

SVM has been utilized to classify multi-temporal sentinel-2 data using one against one multiclass classification technique based on RBF and polynomial kernels. The classification performances on different parameters using different kernel function with optimized parameters on Sentinel-2 imagery of Sept. 2020 (Test case 1) is presented in Tables 3 and 4. In test case 1, it has been observed that the performance of SVM with RBF kernel has produced an OAC of 98.13 as compared to an OAC of 88.88 with the polynomial kernel. While in terms of the KPS parameter, the RBF kernel has 0.9765 as compared to 0.8355 of the polynomial kernel. The performance of the SVM has deteriorated in the case of classifying the road network from such densely populated areas as the road network having a width less than the spatial resolution is not classified as a road. In the case of vegetation class, the RBF kernel has produced 100% but the accuracy of the polynomial kernel is reduced up to 40% due to its poor performance in handling low spectral variable data The road network is generally surrounded by trees and few pixels of the vegetative region are categorized as the road network. While in the case of buildings, land cover and water bodies classes the performance of both kernels remains approximately the same. The classification results of Sentinel-2 imagery obtained in April 2022 are presented in Tables 5 and 6 in which. The SVM kernel produced an overall accuracy of 96.11 as compared to 93.62 for the polynomial kernel. In the case of the KPS parameter, the RBF kernel obtained the value of 0.9513 and as compared to 0.9199 of the polynomial kernel. The low spectral variation effect between road network and vegetative is also reflected in test case 2 as it has the lowest PAC values among all classes. For further investigation of the classification performance of SVM, the imagery of Test Case 1 is classified using the MLC method and the experimental results are shown in Table 7. The OAC and KAS values are less as compared to SVM with RBF kernel but higher than SVM with the polynomial kernel.

Table 7
Error matrix of Test case 1 imagery by MLC

	Road Network	**Vegetation**	**Barren Land**	**Water bodies**	**Residential/Buildings**	**Total**	**User's accuracy**
Road Network	332	22	9	2	4	369	89.97
Vegetation	0	291	0	0	0	291	100
Barren Land	1	0	362	0	24	387	93.54
Water bodies	1	0	0	381	0	382	99.74
Residential/Buildings	0	0	10	0	322	332	96.99
Total	334	313	381	383	350	1761	
Producer's accuracy	99.40	92.97	95.01	99.48	92.00		
Overall Accuracy: 95.85							
Overall kappa 0.9481							

After the analysis of the classification results of imagery of test case 1 and Test case 2 with different techniques, several crucial conclusions can be drawn. Firstly, water bodies are classified with ~ 99% accuracy which shows high classification capability in complex heterogeneous scenes for this particular class. Secondly, the poorest discrimination is against the vegetative class and SVM with RBF has performed as compared to MLC by ~ 10% in Test case 1 imagery and SVM with the polynomial kernel by ~ 60% in Test Case 1 imagery and by ~ 20% in Test Case 2 imagery. Thirdly, SVMs with RBF kernel outclassed SVMs with a polynomial kernel with about 10% enhancement in Test Case 1 and 3% improvement in Test Case 2. This proves the RBF kernel's efficiency to the polynomial kernel in handling heterogeneous complex remote sensing data. Finally, SVMs are found more powerful (~ 3% higher) than the MLC classifier for Test Case 1.

The classification map of the multi-temporal Sentinel imagery of the study area by SVM with RBF and the polynomial kernel is shown in Fig. 2 to Fig. 5. From these classification maps, it is very hard to estimate the classification accuracy visually. Although statistical comparison of different accuracy parameters is presented to support the intuitive comparison between classifications, a change detection investigation can be applied with the results of the classification maps (2020 and 2022) of RBF kernels as it has the highest classification accuracy. The study area is estimated based on % of classified pixels of each class type and a change detection study is applied the results are presented in Table 8. But the change detection period is very short and there exists a variation between spectral resolution of the different periods because Test Case 1 imagery is of post rainy season (autumn) of the study area and Test case 2 imagery is of the spring season.

Table 8
Change detection study of Sentinel-2 imagery of 2020 and 2022

Land Cover Classes	2020 %	2022 %	Change
Road network	29.84	34.93	5.09
Vegetation	6.15	1.1	-5.05
Barren Land	36.84	34.52	-2.32
Water bodies	6.38	11.92	5.54
Residential/Buildings	17.51	20.78	3.27

5. Conclusion

The Sentinel-2 multispectral instrument is quite beneficial for analyzing the earth's surface due to its coverage and provides open source medium resolution data of 10 m. In this work, the performance of SVM kernels (RBF and Polynomial) has been analyzed on multi-temporal Sentinel-2 data of the densely populated urban area. The land cover is classified into different classes namely, road networks, water bodies, vegetation, barren land, and buildings/residential. By performing extensive experiments, it has been observed that the performance of SVM with RBF kernel is best in discriminating the classes having low spectral variation between them. The experimental results of SVM with RBF kernel are further compared with the MLC method. Future research would involve the classification of Sentinel – 2 imagery with a deep learning framework to obtain precise information about land cover and a detailed change detection study having a difference of at least 10 years (of the same type of data and weather season) can be also performed to obtain a better analyze the impact of urbanization.

Declarations

Author's Contribution

Yash Khurana and Pramod Kumar Soni conceived planned Material preparation, and data collection and carried out the experiments. Pramod Kumar Soni and Devershi Pallavi Bhatt contributed to sample preparation and interpretation of the results. The corresponding author took the lead in writing the manuscript. All authors provided critical feedback and helped shape the research, analysis, and manuscript. All authors read and approved the final manuscript.

Availability of Data and Materials

The datasets used in the current study are freely available from earth USGS earth explorer (https://earthexplorer.usgs.gov/) or can be available from the corresponding author upon reasonable request.

Competing interests

The authors have no affiliation with any organization with a direct or indirect financial interest in the subject matter discussed in the manuscript. This manuscript has not been submitted to, nor is under review at, another journal or another publishing venue.

Funding

“No funding was obtained for this study”.

References

1. Abdi AM (2020) Land cover and land use classification performance of machine learning algorithms in a boreal landscape using Sentinel-2 data. GIsci Remote Sens 57:1–20. https://doi.org/10.1080/15481603.2019.1650447
2. Abdollahi A, Bakhtiari HRR, Nejad MP (2018) Investigation of SVM and Level Set Interactive Methods for Road Extraction from Google Earth Images. Journal of the Indian Society of Remote Sensing 46:423–430. https://doi.org/10.1007/s12524-017-0702-x
3. Chen GY, Xie WF (2007) Pattern recognition with SVM and dual-tree complex wavelets. Image and Vision Computing 25:960–966. https://doi.org/10.1016/J.IMAVIS.2006.07.009
4. Cheng G, Wang Y, Gong Y, Zhu F, Pan C (2014) Urban road extraction via graph cuts based probability propagation. In: 2014 IEEE International Conference on Image Processing, ICIP 2014. pp 5072–5076
5. Cohen J (1960) A Coefficient of Agreement for Nominal Scales. Educational and Psychological Measurement 20:37–46. https://doi.org/10.1177/001316446002000104
6. Cortes C, Vapnik V (1995) Support-vector networks. Machine learning 20:273–297
7. Demirel H, Ozcinar C, Anbarjafari G (2010) Satellite Image Contrast Enhancement Using Discrete Wavelet Transform and Singular Value Decomposition. IEEE Geoscience and Remote Sensing Letters 7:333–337. https://doi.org/10.1109/LGRS.2009.2034873
8. Demirel N, Emil MK, Duzgun HS (2011) Surface coal mine area monitoring using multi-temporal high-resolution satellite imagery. International Journal of Coal Geology 86:3–11. https://doi.org/10.1016/j.coal.2010.11.010
9. Dixon B, Candade N (2008) Multispectral landuse classification using neural networks and support vector machines: One or the other, or both? International Journal of Remote Sensing 29:1185–1206. https://doi.org/10.1080/01431160701294661
10. Dutta D, Rahman A, Paul SK, Kundu A (2020) Estimating urban growth in peri-urban areas and its interrelationships with built-up density using earth observation datasets. Ann Reg Sci 65:67–82. https://doi.org/10.1007/s00168-020-00974-8
11. Foody GM (2002) Status of land cover classification accuracy assessment. Remote Sensing of Environment 80:185–201. https://doi.org/10.1016/S0034-4257(01)00295-4
12. Frazier AE, Renschler CS, Miles SB (2012) Evaluating post-disaster ecosystem resilience using MODIS GPP data. International Journal of Applied Earth Observation and Geoinformation 21:43–52. https://doi.org/10.1016/j.jag.2012.07.019
13. Fung T, Ledrew E (1988) The determination of optimal threshold levels for change detection using various accuracy indices. Photogrammetric Engineering & Remote Sensing 54:1449–1454
14. Ghorbanian A, Kakooei M, Amani M, Mahdavi S, Mohammadzadeh A, Hasanlou M (2020) Improved land cover map of Iran using Sentinel imagery within Google Earth Engine and a novel automatic workflow for land cover classification using migrated training samples. ISPRS Journal of Photogrammetry and Remote Sensing 167:276–288. https://doi.org/10.1016/J.ISPRSJPRS.2020.07.013
15. Goldblatt R, Stuhlmacher MF, Tellman B, Clinton N, Hanson G, Georgescu M, Wang C, Serrano-Candela F, Khandelwal AK, Cheng W-H, Balling RC (2018) Using Landsat and nighttime lights for supervised pixel-based image classification of urban land cover. Remote Sens Environ 205:253–275. https://doi.org/https://doi.org/10.1016/j.rse.2017.11.026
16. Huang C, Davis LS, Townshend JRG (2002) An assessment of support vector machines for land cover classification. International Journal of Remote Sensing 23:725–749. https://doi.org/10.1080/01431160110040323

17. Huang H, Coatrieux G, Shu H, Luo L, Roux C (2012) Blind Integrity Verification of Medical Images. IEEE Transactions on Information Technology in Biomedicine 16:1122–1126. https://doi.org/10.1109/TITB.2012.2207435
18. Huang S, Siegert F (2006) Land cover classification optimized to detect areas at risk of desertification in North China based on SPOT VEGETATION imagery. J Arid Environ 67:308–327. https://doi.org/10.1016/j.jaridenv.2006.02.016
19. Isaac E, Easwarakumar KS, Isaac J (2017) Urban landcover classification from multispectral image data using optimized AdaBoosted random forests. Remote Sensing Letters 8:350–359. https://doi.org/10.1080/2150704X.2016.1274443
20. Jebur MN, Mohd Shafri HZ, Pradhan B, Tehrany MS (2014) Per-pixel and object-oriented classification methods for mapping urban land cover extraction using SPOT 5 imagery. Geocarto Int 29:792–806. https://doi.org/10.1080/10106049.2013.848944
21. Johnson BA (2013) High-resolution urban land-cover classification using a competitive multi-scale object-based approach. Remote Sensing Letters 4:131–140. https://doi.org/10.1080/2150704X.2012.705440
22. Lantzanakis G, Mitraka Z, Chrysoulakis N (2020) X-SVM: An Extension of C-SVM Algorithm for Classification of High-Resolution Satellite Imagery. IEEE Transactions on Geoscience and Remote Sensing 1–11. https://doi.org/10.1109/TGRS.2020.3017937
23. Liu R, Song J, Miao Q, Xu P, Xue Q (2016) Road centerlines extraction from high resolution images based on an improved directional segmentation and road probability. Neurocomputing 212:88–95. https://doi.org/10.1016/j.neucom.2016.03.095
24. Magno R, Rocchi L, Dainelli R, Matese A, di Gennaro SF, Chen C-F, Son N-T, Toscano P (2021) AgroShadow: A New Sentinel-2 Cloud Shadow Detection Tool for Precision Agriculture. Remote Sensing 13
25. Mathur A, Foody GM (2008) Multiclass and Binary SVM Classification: Implications for Training and Classification Users. IEEE Geoscience and Remote Sensing Letters 5:241–245. https://doi.org/10.1109/LGRS.2008.915597
26. Miao Z, Shi W, Gamba P, Li Z (2015) An Object-Based Method for Road Network Extraction in VHR Satellite Images. IEEE J Sel Top Appl Earth Obs Remote Sens 8:4853–4862. https://doi.org/10.1109/JSTARS.2015.2443552
27. Milgram J, Cheriet M, Sabourin R (2006) “One Against One” or “One Against All”: Which One is Better for Handwriting Recognition with SVMs? In: Tenth International Workshop on Frontiers in Handwriting Recognition. pp 1–6
28. Mukhopadhyay A, Maulik U (2009) Unsupervised pixel classification in satellite imagery using multiobjective fuzzy clustering combined with SVM classifier. IEEE Transactions on Geoscience and Remote Sensing 47:1132–1138. https://doi.org/10.1109/TGRS.2008.2008182
29. Mukkamala S, Sung AH, Abraham A (2005) Intrusion detection using an ensemble of intelligent paradigms. Journal of Network and Computer Applications 28:167–182. https://doi.org/10.1016/J.JNCA.2004.01.003
30. Naikoo MW, Rihan M, Ishtiaque M, Shahfahad (2020) Analyses of land use land cover (LULC) change and built-up expansion in the suburb of a metropolitan city: Spatio-temporal analysis of Delhi NCR using landsat datasets. Journal of Urban Management 9:347–359. https://doi.org/10.1016/J.JUM.2020.05.004
31. Nizalapur V, Madugundu R, Jha CS (2011) Coherence-based land cover classification in forested areas of Chattisgarh, Central India, using environmental satellite-advanced synthetic aperture radar data. J Appl Remote Sens 5:1–7. https://doi.org/10.1117/1.3557816
32. Norinder U (2003) Support vector machine models in drug design: applications to drug transport processes and QSAR using simplex optimisations and variable selection. Neurocomputing 55:337–346. https://doi.org/10.1016/S0925-2312(03)00374-6
33. Pal M (2008) Multiclass Approaches for Support Vector Machine Based Land Cover Classification. arXiv preprint arXiv:08022411

34. Rana VK, Venkata Suryanarayana TM (2020) Performance evaluation of MLE, RF and SVM classification algorithms for watershed scale land use/land cover mapping using sentinel 2 bands. Remote Sensing Applications: Society and Environment 19:100351. https://doi.org/https://doi.org/10.1016/j.rsase.2020.100351
35. Rottensteiner F, Sohn G, Gerke M, Wegner JD, Breitkopf U, Jung J (2014) Results of the ISPRS benchmark on urban object detection and 3D building reconstruction. ISPRS Journal of Photogrammetry and Remote Sensing 93:256–271. https://doi.org/10.1016/j.isprsjprs.2013.10.004
36. Shekede MD, Murwira A, Masocha M (2015) Wavelet-based detection of bush encroachment in a savanna using multi-temporal aerial photographs and satellite imagery. International Journal of Applied Earth Observation and Geoinformation 35:209–216. https://doi.org/10.1016/J.JAG.2014.08.019
37. Sheykhmousa M, Mahdianpari M, Ghanbari H, Mohammadimanesh F, Ghamisi P, Homayouni S (2020) Support vector machine versus random forest for remote sensing image classification: A meta-analysis and systematic review. IEEE J Sel Top Appl Earth Obs Remote Sens 13:6308–6325
38. Sishodia RP, Ray RL, Singh SK (2020) Applications of remote sensing in precision agriculture: A review. Remote Sens (Basel) 12:3136
39. Spoto F, Martimort P, Drusch M (2012) Sentinel - 2: ESA's optical high-resolution mission for GMES operational services. European Space Agency, (Special Publication) ESA SP 707 SP:25–36
40. Stefanov WL, Ramsey MS, Christensen PR (2001) Monitoring urban land cover change: An expert system approach to land cover classification of semiarid to arid urban centers. Remote Sens Environ 77:173–185. https://doi.org/10.1016/S0034-4257(01)00204-8
41. Steinhausen MJ, Wagner PD, Narasimhan B, Waske B (2018) Combining Sentinel-1 and Sentinel-2 data for improved land use and land cover mapping of monsoon regions. International Journal of Applied Earth Observation and Geoinformation 73:595–604. https://doi.org/10.1016/j.jag.2018.08.011
42. Sumer E, Turker M (2013) An adaptive fuzzy-genetic algorithm approach for building detection using high-resolution satellite images. Comput Environ Urban Syst 39:48–62. https://doi.org/10.1016/j.compenvurbsys.2013.01.004
43. Wang M, Wan Y, Ye Z, Lai X (2017) Remote sensing image classification based on the optimal support vector machine and modified binary coded ant colony optimization algorithm. Information Sciences 402:50–68. https://doi.org/10.1016/j.ins.2017.03.027
44. Xu Y, Du B, Zhang L, Cerra D, Pato M, Carmona E, Prasad S, Yokoya N, Hänsch R, Saux B le (2019) Advanced Multi-Sensor Optical Remote Sensing for Urban Land Use and Land Cover Classification: Outcome of the 2018 IEEE GRSS Data Fusion Contest. IEEE J Sel Top Appl Earth Obs Remote Sens 12:1709–1724. https://doi.org/10.1109/JSTARS.2019.2911113
45. Yang X (2011) Parameterizing support vector machines for land cover classification. Photogramm Eng Remote Sensing 77:27–38. https://doi.org/10.14358/pers.77.1.27
46. Zhu Z, Woodcock CE, Rogan J, Kellndorfer J (2012) Assessment of spectral, polarimetric, temporal, and spatial dimensions for urban and peri-urban land cover classification using Landsat and SAR data. Remote Sens Environ 117:72–82. https://doi.org/10.1016/J.RSE.2011.07.020
47. Census of India. https://censusindia.gov.in/census.website/. Accessed 27 Sep 2022
48. earthexplorer. https://earthexplorer.usgs.gov/. Accessed 27 Sep 2020

Figures

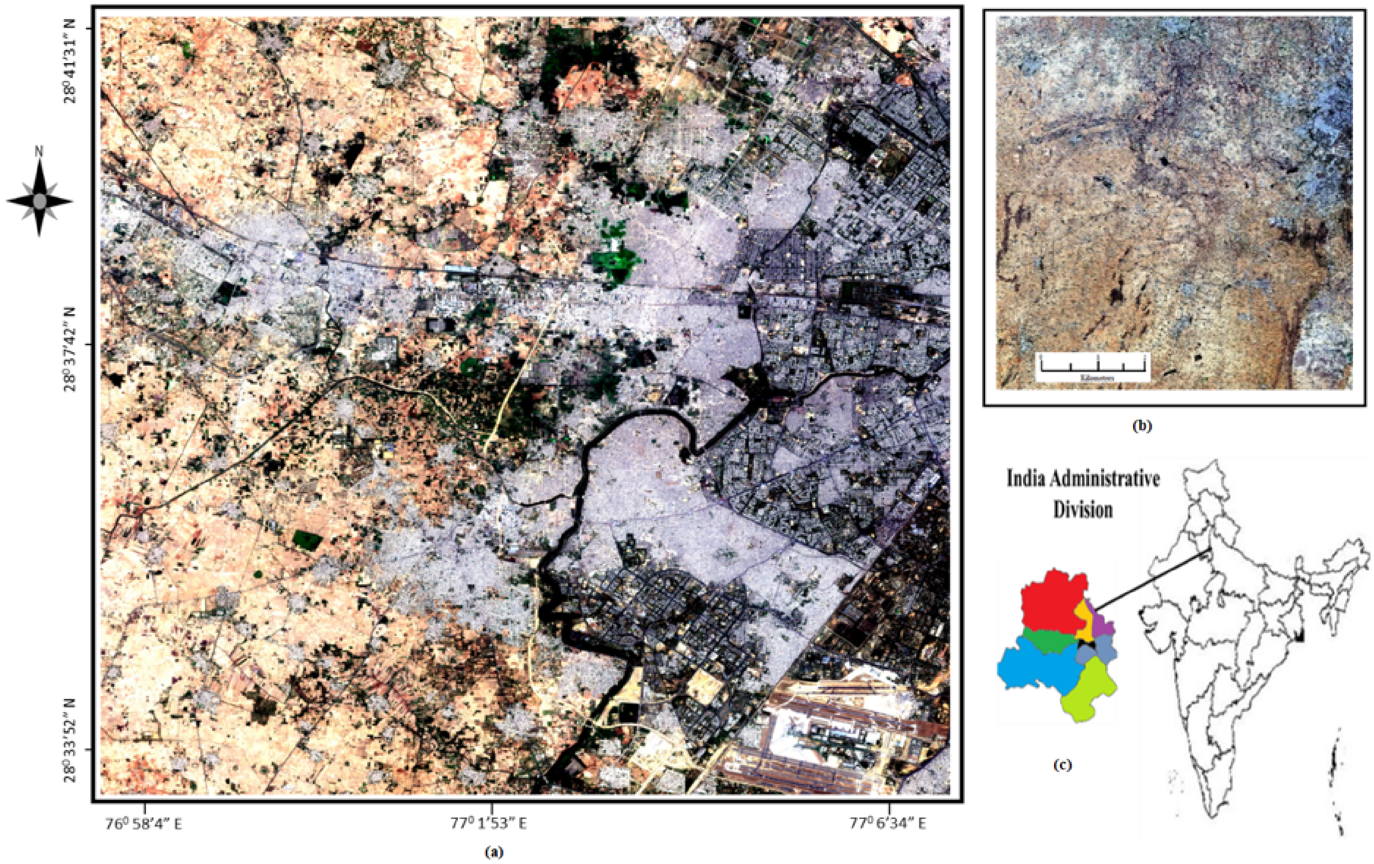

Figure 1

(a) Extracted Sentinel -2 imagery of the study area (b) Orginal data obtained from Sentinel-2 satellite (c) Geographical location of the study area

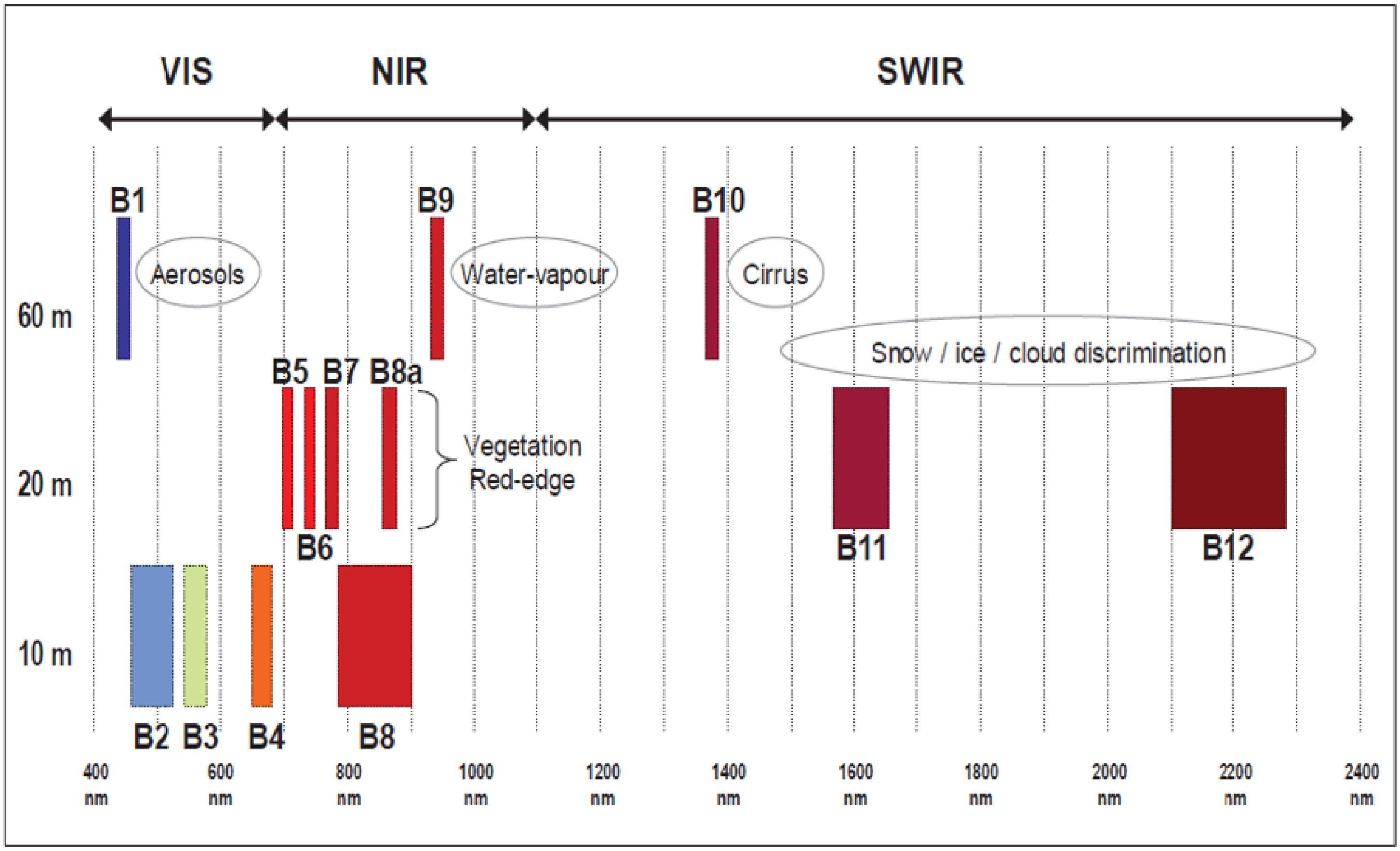

Figure 2

Relationship between spatation resolution and spectral bands

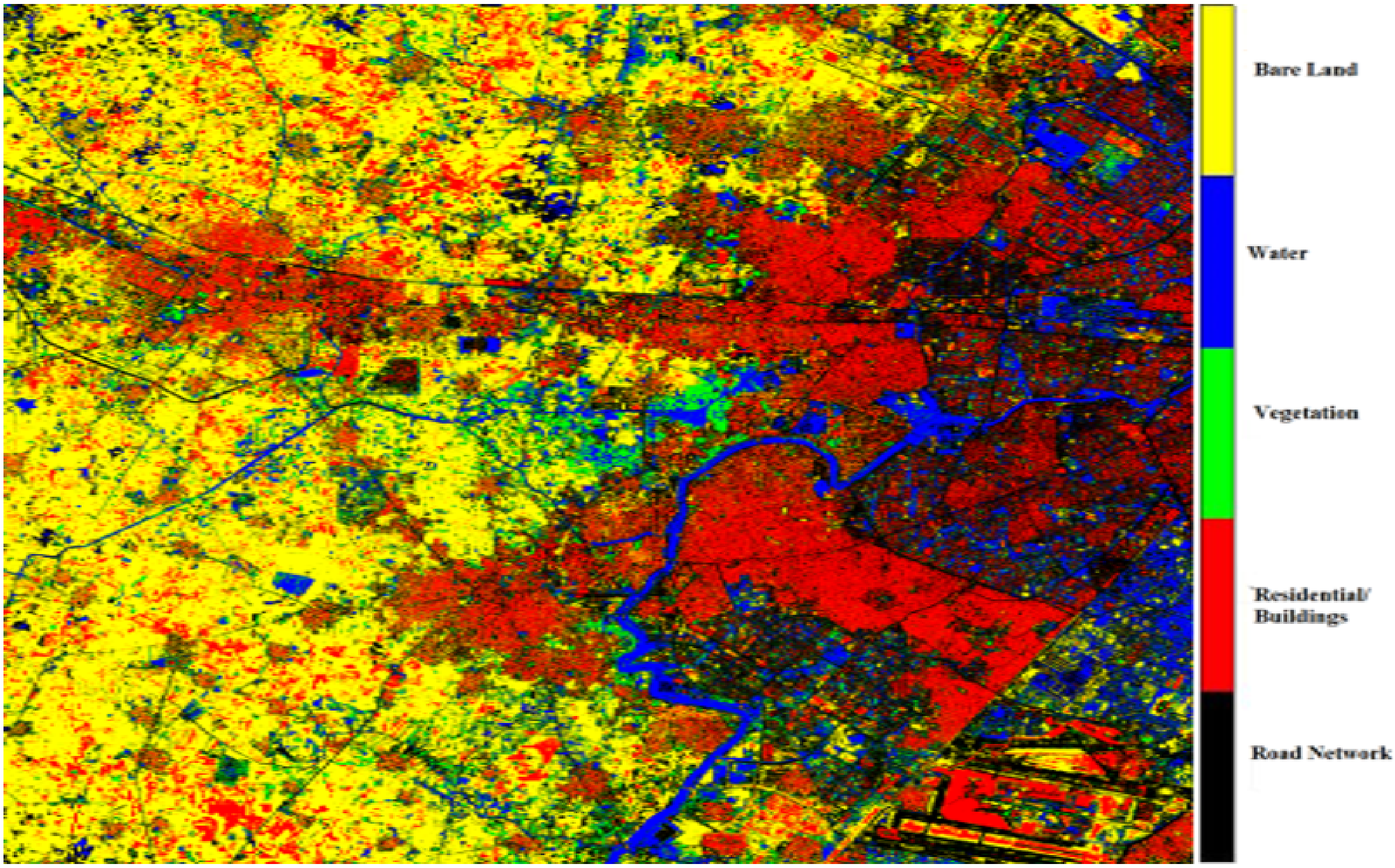

Figure 3

Figure 2. Classification map of Test Case 1 using SVM with RBF kernel

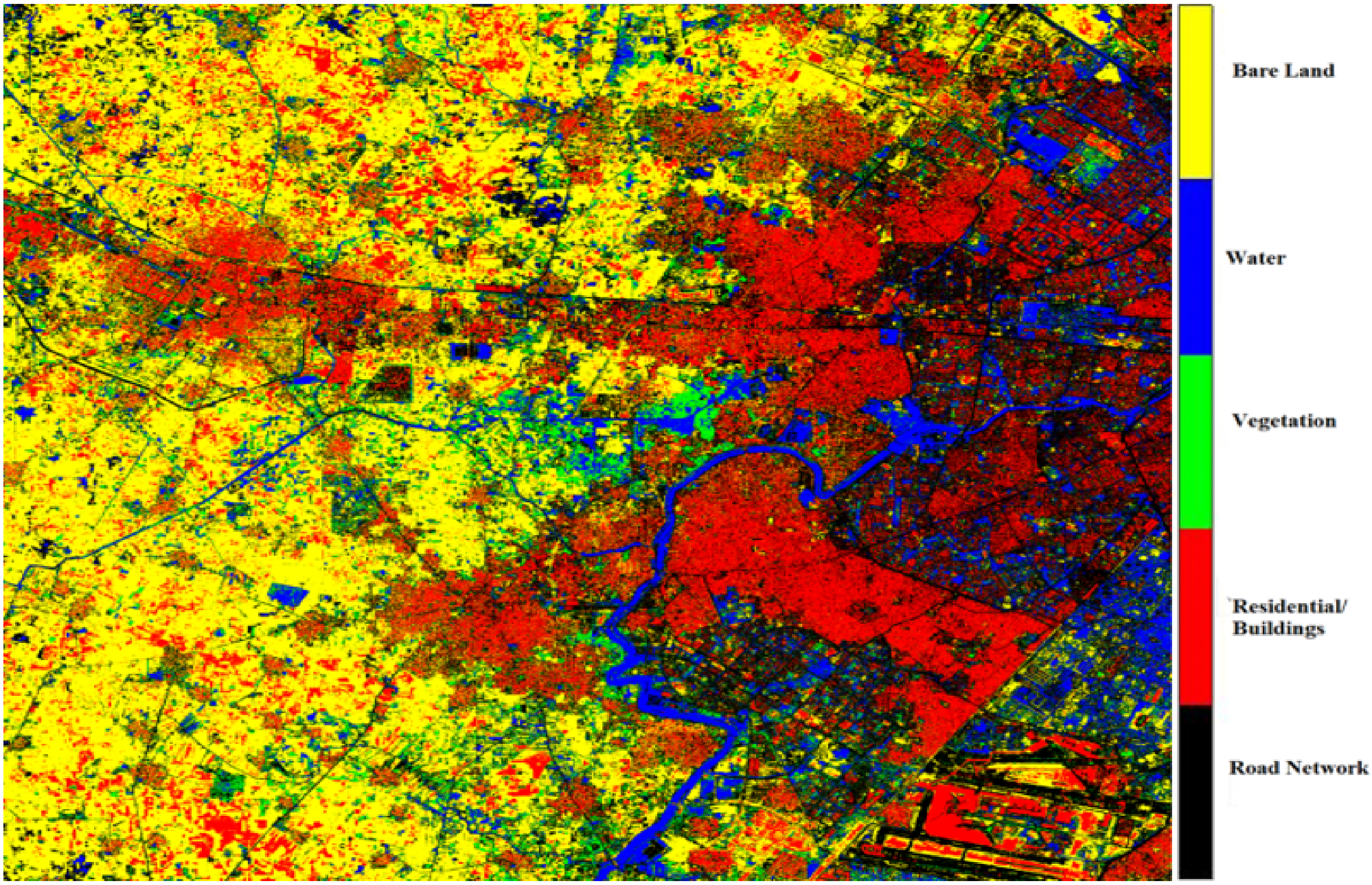

Figure 4

Figure 3 Classification map of Test Case 1 using SVM with polynomial kernel

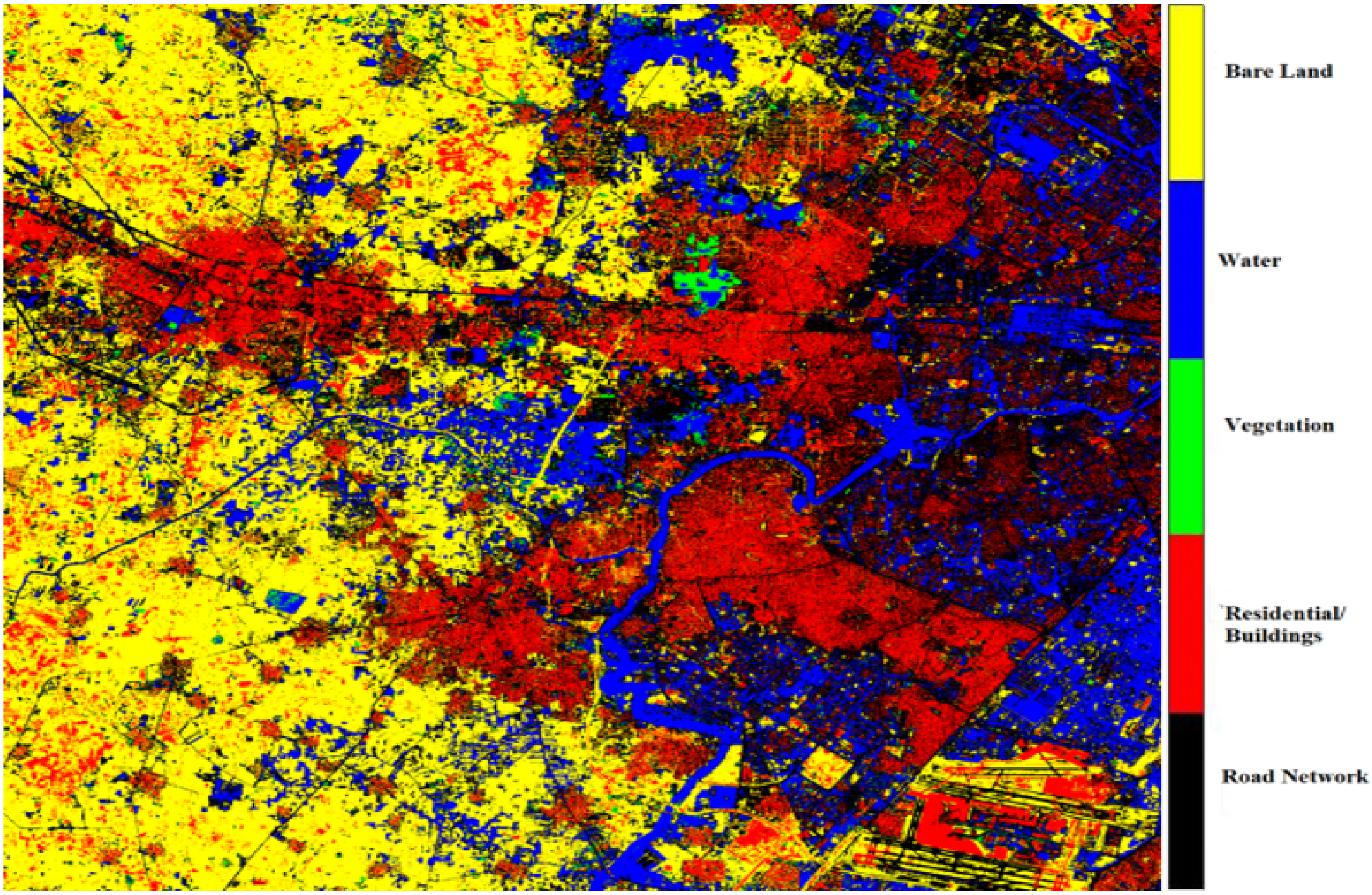

Figure 5

Figure 4. Classification map of Test Case 2 using SVM with RBF kernel

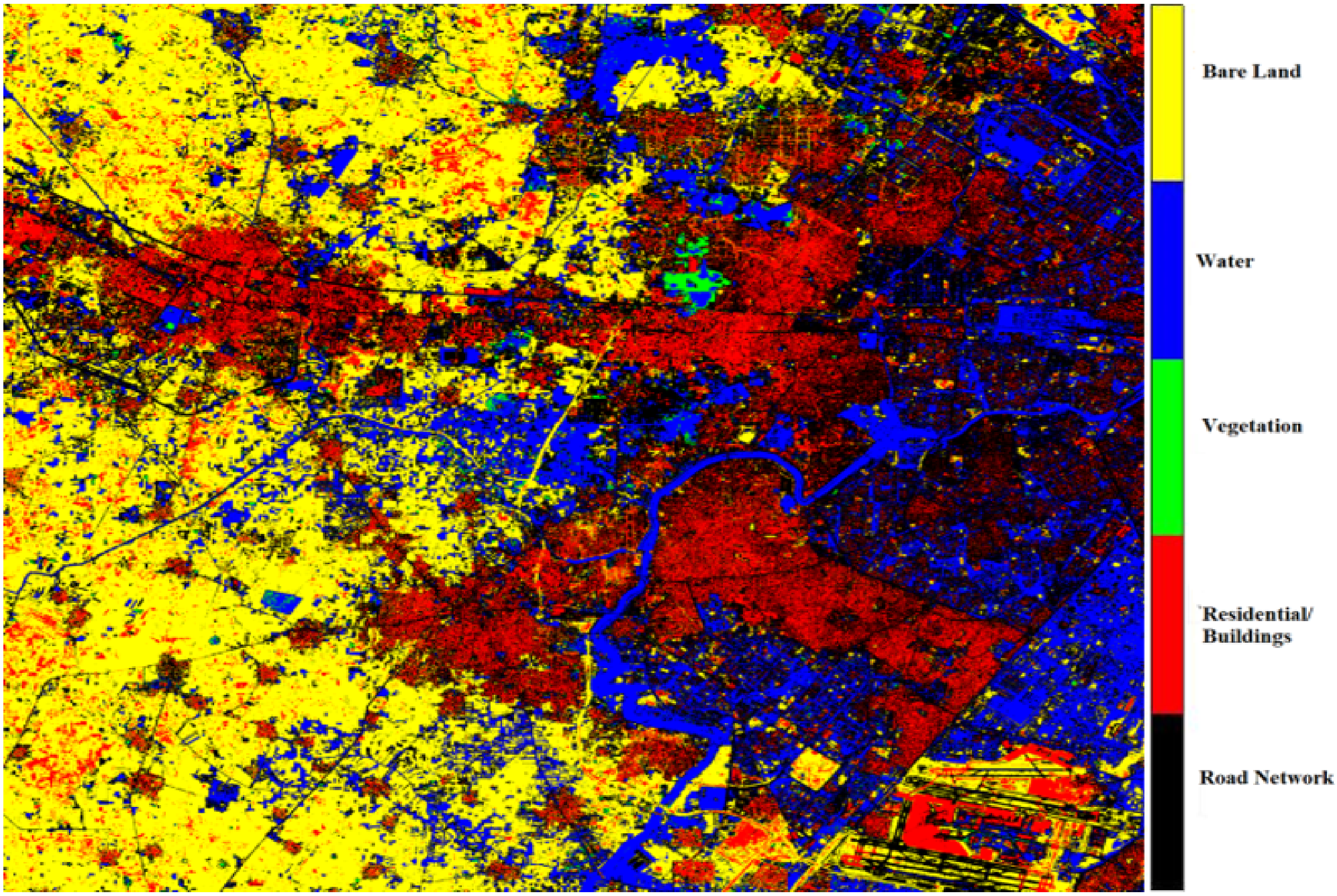

Figure 6

Figure 5. Classification map of Test Case 1 using SVM with polynomial kernel